Magnetic frustration in the high-pressure Mn2MnTeO6 (Mn3TeO6–II) double perovskite.

Angel M. Arevalo-Lopez, Elena Solana-Madruga, Cintli Aguilar-Maldonado, Clemens Ritter, Olivier Mentré, Paul Attfield

Journal Name

COMMUNICATION

Magnetic frustration in the high-pressure Mn_2MnTeO_6 (Mn_3TeO_6–II) double perovskite.

Received 00th January 20xx,
Accepted 00th January 20xx

DOI: 10.1039/x0xx00000x

www.rsc.org/

Ángel M. Arévalo-López[a]*, Elena Solana-Madruga,[b] Cintli Aguilar-Maldonado,[a] Clemens Ritter,[c] Olivier Mentré,[a] and J.Paul Attfield[b]*

A new double perovskite Mn_2MnTeO_6 has been obtained by high pressure phase transformation of a corundum-related precursor. It is antiferromagnetic below 36 K and develops a magnetic structure with magnetic moments of 4.8 μ_B and 3.8 μ_B for Mn^{2+} at the A and B sites respectively. This new polymorph accounts for a recently reported decrease in the bandgap of Mn_3TeO_6 under pressure that may lead to useful light-harvesting properties.

The ABO_3 perovskite structure has proven to be very versatile, since it can accommodate several cations at both A and B sites. The consequent accessibility to a wide range of magnetic and electrical properties have attracted much attention. Perovskites show increasing distortion with decreasing ionic radius of the A-site cation, down to tolerance factors $t = (r_A+r_O)/(\sqrt{2}(r_B+r_O))$ of 0.75, where r_A, r_B and r_O are the ionic radii of the A, B and O ions[1]. However, the use of high pressures enables small cations such as Mn^{2+} (r = 0.96 Å)[2] to be accommodated at the A-sites, allowing complex electronic and magnetic interactions. For example $Mn^{2+}V^{4+}O_3$ perovskite shows the coexistence of localized d^5 Mn^{2+} and itinerant d^1 electron V^{4+} cations[3]. Further variety is achieved in high pressure double perovskites (DPvs) $Mn_2BB'O_6$ with ordering of two cations on the B sites; Mn_2BSbO_6 (B = Sc, Cr, and Fe)[4-6], Mn_2BReO_6 (B = Mn, Fe and Co)[7-9] and $Mn_2(Fe_{0.8}Mo_{0.2})MoO_6$.[10]
Tellurium based oxides M_2MTeO_6 (M = Mn, Co and Ni) have structures based on the corundum arrangement at ambient pressure (see Supplementary Figure 1) and show a variety of complex magnetic orders. Mn_3TeO_6-I crystallises in the Mg_3TeO_6-type structure.[11] Below 24 K it shows the coexistence of an elliptical helix and a sinusoidal spin density wave, both being incommensurate with the crystal structure. This phase has shown a dielectric response below 21 K and so is a type-II multiferroic[12]. Co_3TeO_6 has 5 independent Co sites, providing a rich magnetic phase diagram[13] and Ni_3TeO_6 is a non-hysteretic colossal magnetoelectric material with a collinear antiferromagnetic (AFM) structure stabilised on stacked honeycomb layers[14].
A recent study of light-harvesting properties of Mn_3TeO_6-I discovered an irreversible 39% bandgap reduction during in-situ measurements under pressure[15]. We have explored the possibility of transforming ambient pressure Mn_3TeO_6-I phase into a recoverable double perovskite using high pressure and high temperature conditions, and we report here the new double perovskite Mn_2MnTeO_6, which is likely to be responsible for the reported bandgap engineering.
Mn_3TeO_6-I, prepared at 1270 K by the solid state synthesis method of reference 11 was packed into a Pt capsule, pressed at 8 GPa and heated at 1173 K using a Walker-type module in a multianvil press. After 20 minutes, the temperature was quenched and the pressure was slowly released. Synchrotron X-ray diffraction (SXRD) powder data were collected at room temperature using the BL04 beamline at ALBA, Barcelona. Neutron powder diffraction (NPD) data were taken on 6 combined high pressure samples (≈ 120 mg) at 50 K, 1.5 K and several intermediate temperatures using the D1B beamline at the ILL, Grenoble. Zero-field cooled and field cooled (ZFC and FC) magnetic susceptibilities and a magnetisation-field loop at 2 K were measured using a PPMS Dynacool from Quantum Design.
Preliminary laboratory X-ray diffraction evidenced the transition from Mn_3TeO_6-I into a new double perovskite, Mn_3TeO_6-II. This was found to have a monoclinic $P2_1/n$ rock-salt B-site ordered DPv structure from Rieveld fitting of 300 K SXRD data (Fig. 1a). A few % of δ-Mn_3O_4 ($CaMn_2O_4$-type) and Pt from the capsule are included in the refinements. The SXRD results are summarised in Table 1 and the structure is shown in Fig. 1b.

[a] Univ. Lille, CNRS, Centrale Lille, ENSCL, Univ. Artois, UMR 8181 - UCCS - Unité de Catalyse et Chimie du Solide, F-59000 Lille, France. *angel.arevalo-lopez@univ-lille.fr
[b] Centre for Science at Extreme Conditions (CSEC) and School of Chemistry, The University of Edinburgh. EH9 3FD, U.K. * j.p.attfield@ed.ac.uk
[c] Institut Laue-Langevin, Avenue des Martyrs 71, 32042, Grenoble Cedex, France.
† Data that support the findings of this study have been deposited at https://datashare.is.ed.ac.uk/handle/10283/838.
‡ Electronic Supplementary Information (ESI) available: supporting figures and tables. See DOI: 10.1039/x0xx00000x

Antisite disorder between Mn_B and Te positions was checked but no mixing was found within error showing that Mn_3TeO_6-II is fully cation-ordered. The refined structural model shows that the Mn_BO_6 octahedra are distorted while TeO_6 octahedra are more regular (Table 1). Octahedral tilts ~20^0 are comparable to those for other $Mn_2BB'O_6$ double perovskites and reflect the significant distortion in agreement with the small t-value (t = 0.8) for this high pressure polymorph.

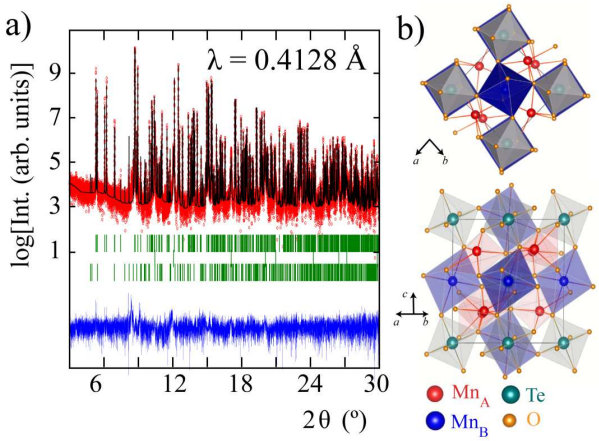

Figure 1. Rietveld fit (a) of the DPv structure of Mn_2MnTeO_6 (b) from 300 K SXRD data. Second and third rows of Bragg tick marks are minor amounts of Pt from the capsule (2.2(1) %) and δ-Mn_3O_4 (1.9(1) %).

Table 1. Atomic positions and main interatomic distances and bond angles from the Rietveld fit of 300 K SXRD data. S.G. $P2_1/n$, a = 5.29370(1) Å, b = 5.45203(1) Å, c = 7.80894(1) Å, β = 89.62514(5) º.

Site	x	y	z	Biso (Å^2)	Occ
Te (2a)	0	0	0	0.43(1)	0.5
Mn_B (2b)	0.5	0.5	0	0.56(2)	0.5
Mn_A (4e)	0.4887(2)	0.0475(1)	0.2397(1)	0.66(2)	1
O1 (4e)	0.1677(8)	0.2784(7)	0.0808(6)	0.31(5)	1
O2 (4e)	0.7106(8)	0.1745(8)	-0.0520(5)	0.31(5)	1
O3 (4e)	0.8794(7)	0.9244(7)	0.2215(5)	0.31(5)	1

d_{M-O} (Å)		<M-O-M> (º)	
2x (Mn_B-O1)	2.308(4)	Mn_B-O1-Te	136.2(3)
2x (Mn_B-O2)	2.133(5)	Mn_B-O2-Te	144.9(3)
2x (Mn_B-O3)	2.308(4)	Mn_B-O3-Te	137.0(3)
<Mn_B-O>	2.249(6)		
2x (Te-O1)	1.870(5)	Mn_A-O1-Mn_B	96.5(1)
2x (Te-O2)	1.851(5)	Mn_A-O2-Mn_B	109.6(2)
2x (Te-O3)	1.885(4)	Mn_A-O3-Mn_B	98.7(1)
<Te-O>	1.868(5)		
2x Mn_A-O1	2.188(5) 2.458(5)	ϕ	21.5^0
3x Mn_A-O2	2.179(5) 2.648(5) 2.660(5)	θ	19.7^0
2x Mn_A-O3	2.178(5) 2.192(4)	Δ[Mn_BO_6]	2.30*10^{-3}
<Mn_A-O>	2.358(4)	Δ[TeO_6]	1.04*10^{-4}

Octahedral distortions calculated from $\Delta[MO_6]=(1/n)*\Sigma(d_i-d_{av})^2/d_{av}$. Tilt angles along [001] ϕ and [110] θ are calculated from (180-<M-O-M>)/2. R_p = 16.8%, R_{wp} = 21.9%, R_f = 5.34%, R_B = 7.50%, χ^2 = 2.22 %.

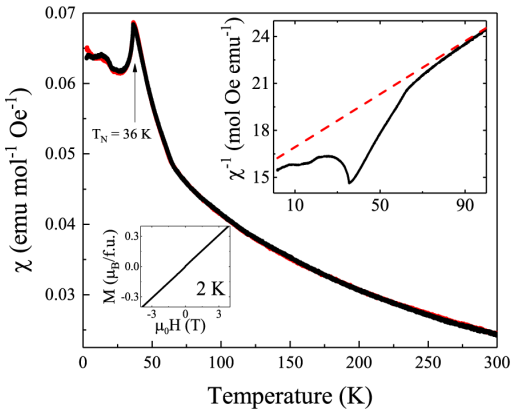

Figure 2. ZFC (black) and FC (red) magnetic susceptibility of Mn_2MnTeO_6 Insets show the reciprocal susceptibility with C-W from high temperature (red dashed line) (right) and the field dependent magnetisation at 2K (left).

ZFC and FC magnetic susceptibilities were measured under an external field of 500 Oe (Figure 2). They show a single antiferromagnetic transition at T_N = 36(0.5) K. A Curie-Weiss fit to the inverse susceptibility in the 100 - 300 K temperature range gives μ_{eff} = 5.6 μ_B/Mn^{2+}, in good agreement with the theoretical value of 5.92 μ_B for spin only Mn^{2+} (S = 5/2). The large negative Weiss constant θ = -183(1) K indicates predominant antiferromagnetic interactions, and the linear dependence of magnetisation on applied field at 2 K (left inset in Figure 2), demonstrates the absence of a ferromagnetic component to the low temperature order. The upturn of the susceptibility observed below 25 K may be due to traces of the Mn_3TeO_6-I phase (T_N = 24 K).

Rietveld fits to the NPD data collected at D1B at 50 K and 1.5 K are shown in Figure 3a. The large difference between neutron scattering lengths for Mn (-3.73 fm) and Te (5.80 fm) appear ideal to test for antisite disorder, thus the refinements confirmed the well-ordered structural model obtained from SXRD. Oxidation states estimated from BVS calculations on the 50 K NPD model are 2.1, 1.7 and 6.0 for Mn_A, Mn_B and Te sites respectively, demonstrating that the charge distribution is $Mn_2^{2+}Mn^{2+}Te^{6+}O_6$.

Prominent magnetic peaks observed below T_N can be indexed with the k = [½ 0 ½] propagation vector. The magnetic symmetry analysis was performed using the BasIreps tool implemented in the Rietveld refinement program FullProf Suite[16]. The resulting irreducible representations (Ireps) are summarised in Table S1 in the ESI and all four simple possible models were tested. The best fit is when both A- and B-site Mn spins follow Irep Γ_4 and can be refined independently (R_B = 6.60%, R_f = 8.54%, R_{Mag} = 10.1%, χ^2 = 1.233 for T = 1.5 K). The 1.5 K – 50 K difference pattern containing only magnetic intensity is shown as an inset in the lower panel of Figure 3a and magnetic refinement details are shown in ESI and Table S2.

The magnetic structure of Mn_2MnTeO_6-II, depicted in Figure 3b, can be described as *ab* layers of Mn_A spins AFM coupled with Mn_B spins perpendicular to the *a* direction in the magnetic unit cell. These layers are separated by diamagnetic TeO_6 octahedra, stacked AFM along the *c* direction and with the spins confined in the *ac* plane. The 90° superexchange Mn_A-O-Mn_B d^5-d^5 interactions are assumed to be the dominant ones (see Table 1), and satisfy the Goodenough-Kanamori-Anderson rules (GKA).[17] The refined ordered magnetic moments at 1.5 K converge to μ_A = 4.8(6) μ_B and μ_B = 3.9(1) μ_B for A- and B-site Mn^{2+} respectively. The refined value for Mn_A agrees well with the expected ordered magnetic moment of 5 μ_B for Mn^{2+}, while the reduced value obtained for the Mn_B sublattice reflects some frustration present in the system, the later also supported by the ratio $f = |\theta|/T_N \sim 5$.

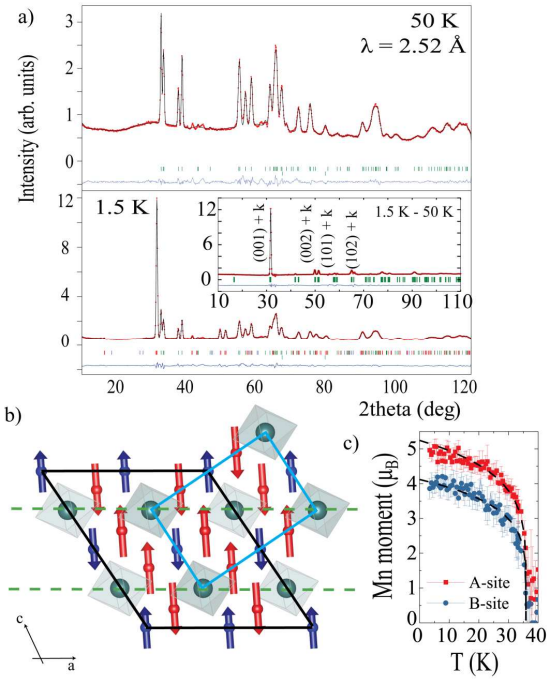

Figure 3. a) Rietveld fits of the nuclear and magnetic structures to the 50 K (top) and 1.5 K (bottom) NPD data. The right inset shows the fit of the magnetic model to the 1.5 K – 50 K difference pattern. b) *ac* plane of the magnetic structure of Mn_2MnTeO_6 with Mn_A and Mn_B spins as red and blue arrows respectively. Magnetic unit cell t is delimited with a black line and related to the crystallographic cyan one via the transformation matrix: [(1 0 -1), (0 -1 0), (-2 0 0)] with an origin shift of (0, 0, 1/2) and magnetic space group P_c2_1/n (14.80). Green dashed lines show the AFM planes described in the text. c) Thermal evolution of the Mn^{2+} magnetic moments and fit to the critical law (dashed black line) as described.

The magnetic model was used to fit the NPD scans at intermediate temperatures giving the evolution of the magnetic moments at both sites, as shown in Fig. 3c. Their fit by the critical law $\mu(T) = \mu(0)*[1-(T/T_N)]^\beta$ in the $(T_N / 2) < T < T_N$ temperature range led to the parameters T_N = 35.8(1) K and $\beta \approx 0.19(1)$, confirming a simultaneous order of both sublattices, in agreement with magnetisation measurements. The small β value suggests a reduced dimensionality, being close to the expected value of 0.23 for a 2D-XY model[18] and agreeing with the refined magnetic structure with spin directions confined into the *ac* plane.

In this context, the comparison with related high-pressure double perovskites $Mn_2BB'O_6$ is remarkable. Table 2 summarises the main features of their magnetic behaviours, which suggests the essential role of the diamagnetic B' cation on the frustrated B-site magnetic moments of these compounds as detailed below. Mn_2MnTeO_6, Mn_2MnReO_6 and Mn_2CoReO_6 are the only $Mn_2BB'O_6$ compounds reported to stabilise a DPv structure with divalent B and hexavalent B' cations. The highest magnetic frustration is observed in Mn_2MnTeO_6 and is released in Mn_2BReO_6 by the presence of the paramagnetic cation Re^{6+}, which enables further superexchange pathways within the B sublattice and consequently increases T_N. Both Mn_2CoReO_6 and Mn_2MnReO_6 become ordered around 100 K into almost perpendicular AFM A and B sublattices with k = [½ ½ 0] and with reduced moments in B.[9,7] The isoelectronic Mn^{2+} cations at A and B sites in Mn_2MnReO_6 give rise to magnetoelastic effects that prompt Re magnetic ordering at lower temperatures than the Mn (f = 1.4). However, in Mn_2CoReO_6 with Co^{2+} in a high spin state, some GKA paths are blocked and it recovers some frustration increasing f up to 3.6. In Mn_2FeReO_6 the strong coupling between Fe^{3+} (d^5) and Re^{5+} (d^2) leads to a ferrimagnetic ordering on the B/B'-sites at high temperatures into a simple k = [0 0 0] magnetic structure (f = 0.9).[8] Likewise, $Mn_2Fe_{0.8}Mo_{0.2}MoO_6$ shows almost no frustration (f = 0.3) due to the B-sublattice disordering of cations and the presence of Mo in a 4+ and 5+ oxidation states.

Our comparison has to include compounds of type Mn_2BSbO_6 (B = Sc, Cr and Fe) due to the presence of a diamagnetic B' cation as in Mn_2MnTeO_6. All of them achieve high degrees of magnetic frustration with transitions lower than 60 K. B = Sc, where only Mn^{2+} at the A sites are paramagnetic, has a strong frustration (f = 4.3) with AFM order at 22 K into a simple collinear magnetic structure with k = [0 0 0].[4] B = Cr^{3+} shows the closest magnetic structure to that of Mn_2MnTeO_6, with k = [½ 0 ½] and AFM d^5-d^3 A-O-B superexchange interactions at 90°.[5]**Erreur ! Signet non défini.** The weaker nature of these interactions compared to the d^5-d^5 Mn^{2+}_A-O-Mn^{2+}_B of Mn_2MnTeO_6, justifies the slightly lower frustration of Mn_2CrSbO_6. Finally, Mn_2FeSbO_6 is isoelectronic to Mn_2MnTeO_6 with both Mn^{2+} and Fe^{3+} d^5 cations. Mn_2FeSbO_6 presents an incommensurate helical magnetic structure with k = [0 0.426 0].[6] The origin of this difference is that the exchange integral for Fe^{3+} is much larger than that for Mn^{2+},[19] inducing strong competitions between AFM d^5-d^5 A-O-B and A-O-A interactions, thus frustrating the compound into a helical magnetic structure. In the case of Mn^{2+} the larger difference between these interactions, prevents the rotation of the spins and the release of the strong magnetic frustration, see Supporting Information for the interplays between A-A, B-B and A-B with frustrated topologies.

Finally, Mn_3TeO_6 has been recently reported as a promising light-harvesting material due to an irreversible pressure-

induced phase transition occurring at 16-18 GPa, where an energy bandgap reduction of $\Delta E_{gap} \approx 1$ eV is observed.[15] Our experimental plots of the Kubelka-Munk function of the UV-VIS reflectance spectra in Figure 4 show a $\Delta E_{gap} \approx 0.8$ eV reduction from the Mn_3TeO_6 precursor (E_{gap} = 2.6 eV) to the Mn_2MnTeO_6 perovskite (E_{gap} = 1.8 eV) and we conclude that this is very probably the phase observed in the high pressure measurements. The change in connectivity from edge- to corner-shared octahedra between both polymorphs explains the decrease in the bandgap in the double perovskite.[20]

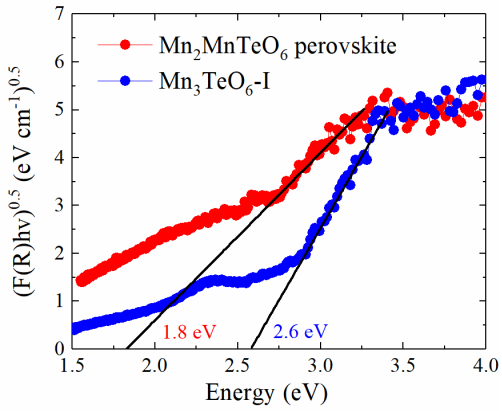

Figure 4. Kubelka-Munk plots (for an indirect bandgap) - for Mn_3TeO_6-I and the Mn_2MnTeO_6 high-pressure double perovskite polymorph, both measured at ambient pressure and temperature.

Table 2. Main features of the magnetic behaviour for $Mn_2BB'O_6$ double perovskites, including, electronic configuration of B and B' cations, transition temperature, Weiss constant (θ), frustration index ($f = |\theta|/T_N$) and propagation vector (k).

B	B'	d_B		$d_{B'}$	T_N/T_C (K)	θ	f	k
		t_{2g}	e_g					
Sc	Sb	0	0	10	22	94	4.3	0 0 0[4]
Mn	Te	3	2	10	36	183	5.1	½ 0 ½*
Cr	Sb	3	0	10	55	220	4.0	½ 0 ½[5]
Fe	Sb	3	2	10	60	180	3.0	0 k_y 0[6]
Co	Re	5	2	1	94	26	3.6	½ ½ 0[9]
Mn	Re	3	2	1	109	147	1.4	½ ½ 0[7]
$Fe_{0.8}Mo_{0.2}$	Mo	3	2	1	194	50	0.3	0 0 0[10]
Fe	Re	3	2	2	520	452	0.9	0 0 0[8]

*This work

In conclusion, a new DPv Mn_2MnTeO_6 has been prepared by high-pressure high-temperature transformation of the rhombohedral polymorph. Due to the large charge and size difference between Mn^{2+} and Te^{6+}, Mn_2MnTeO_6 shows a fully ordered B/B' rock-salt type DPv structure. It is AFM below T_N = 36 K and it develops a complex magnetic structure with ordered magnetic moments of 4.8 (1) μ_B and 3.8 (1) μ_B at the A and B sites respectively. The magnetic structure describes AFM *ab* layers of A- and B-site spins, AFM coupled along the *c* axis, with the spins confined in the *ac* plane. Mn_2MnTeO_6 shows the highest frustration index among the A-site manganites with DPv structure. Replacement by non-magnetic B' cations proves to be a way to enhance the frustration and may be used as tuning parameter in partial B' substitutions. Formation of this DPv polymorph accounts for the previously reported bandgap reduction under pressure.

We thank EPSRC for support, and ALBA and the ILL for beamtime provided at BL04 and D1B beamlines respectively. AMAL thanks a Marie-Słodowska Individual Fellowship in the Horizon 2020 research and innovation programme under grant agreement 750971 ("KISS ME") and the ANR-AMANTS (19-CE08-0002-01) and LOVE-ME (16-CE08-0023) projects. CAM thanks CONACyT-Mexico for a post-doctoral fellowship (CVU:350841). Chevreul Institute (FR 2638), Region Hauts-de-France, and FEDER are acknowledged for funding the X-ray diffractometers and the PPMS magnetometer.

Conflicts of interest. There are no conflicts to declare.

Notes and references

[1] V.M. Goldschmidt, *Mat-Naturu Kl* 1926, **2**, 117.
[2] R.D. Shannon, C.T. Prewitt, *Acta Cryst.B.* 1969, **25**, 925.
[3] M. Markkula, A.M. Arevalo-Lopez, A. Kusmartseva, J.A. Rodgers, C. Ritter, H. Wu, J.P. Attfield, *Phys. Rev. B.* 2011, **84**, 094450.
[4] E. Solana-Madruga, A.J. Dos santos-García, A.M. Arévalo-López, D. Ávila-Brande, C. Ritter, J.P. Attfield, R. Sáez-Puche, *Dalton Trans.*, 2015, **44**, 20441.
[5] A.J. Dos santos-García, E. Solana-Madruga, C. Ritter, D. Ávila-Brande, O. Fabelo, R. Sáez-Puche, *Dalton Trans.*, 2015, **44**, 10665.
[6] A.J. Dos santos-García, C. Ritter, E. Solana-Madruga, R. Sáez-Puche, *J. Phys.: Condens. Matter*, 2013, **25**, 206004.
[7] A.M. Arévalo-López, F. Stegemann, J.P. Attfield, *Chem. Commun.* 2016, **52**, 5558.
[8] A.M. Arévalo-López, G.M. McNally, J.P. Attfield, *Angew. Chem. Int. Ed.* 2015, **54**, 12074.
[9] C.E. Frank, E.E. McCabe, F. Orlandi, P. Manuel, X. Tan, Z. Deng, M. Croft, V. Cascos, T. Emge, H.L. Feng, S. Lapidus, C. Jin, M.X. Wu, M.R. Li, S. Ehrlich, S. Khalid, N. Quackenbush, S. Yu, D. Walkerk, M. Greenblatt, *Chem. Commun.*, 2019, **55**, 3331.
[10] M.-R. Li, P.W. Stephens, M. Croft, Z. Deng, W. Li, C. Jin, M, Retuerto, J.P. Hodges, C.E. Frank, M.X. Wu, D. Walker, M. Greenblatt, *Chem. Mater.,* 2018, **30**, 4508.
[11] S.A. Ivanov, P. Nordblad, R. Mathieu, R. Tellgren, C. Ritter, N.V. Golubko, E.D. Politova, M. Weile, *Mat. Res. Bull.* 2011, **46**, 1870.
[12] S.A. Ivanov, C. Ritter, P. Nordblad, R. Tellgren, M. Weil, V. Carolus, T. Lottermoser, M. Fiebig, R. Mathieu, *J. Phys. D: Appl. Phys.* 2017, **50**, 085001.
[13] S.A. Ivanov, R. Tellgren, C. Ritter, P. Nordblad, R. Mathieu, G. André, E.D. Politova, M. Weil, *Mat. Res. Bull.* 2012, **47**, 63.
[14] Y.S. Oh, S. Artyukhin, J.J. Yang, V. Zapf, J.W Kim, D. Vanderbilt, S.-W. Cheong, *Nat. Comm.* 2014, 4201.
[15] L. Liu, H. Skogby, S. Ivanov, M. Weil, R. Mathieu, P. Lazor, *Chem. Comm.* 2019, Advance Article.
[16] J. Rodriguez-Carvajal, *Physica B*, 1993, **192**, 55.
[17] J.B. Goodenough, *Magnetism and the chemical bond*. Wiley, New York, 1963.
[18] A. Taroni, S.T. Bramwell, P.C.W. Holsworth, *J. Phys.: Condens. Matter*, 2008, **20**, 275233.
[19] P. W. Anderson, *Solid State Phys.* 1963, **14**, 99.
[20] M.E. Kamminga, G.A.de Wijs, R.W.A.Havenith, G.R. Blake, T.T.M. Palstra, *Inorg. Chem.* 2017, **56**, 8408.